Structure, Vol. 11, 961–972, August, 2003, ©2003 Elsevier Science Ltd. All rights reserved. DOI 10.1016/S0969-2126(03)00153-9

The 1.14 Å Crystal Structure of Yeast Cytosine Deaminase: Evolution of Nucleotide Salvage Enzymes and Implications for Genetic Chemotherapy

Gregory C. Ireton,[1] Margaret E. Black,[2] and Barry L. Stoddard[1,*]
[1]Fred Hutchinson Cancer Research Center and Graduate Program in Molecular and Cell Biology
University of Washington
1100 Fairview Avenue North A3-023
Seattle, Washington 98109
[2]Department of Pharmaceutical Sciences
College of Pharmacy
Washington State University
Pullman, Washington 99164

Summary

Cytosine deaminase (CD) catalyzes the deamination of cytosine and is only present in prokaryotes and fungi, where it is a member of the pyrimidine salvage pathway. The enzyme is of interest both for antimicrobial drug design and gene therapy applications against tumors. The structure of *Saccharomyces cerevisiae* CD has been determined in the presence and absence of a mechanism-based inhibitor, at 1.14 and 1.43 Å resolution, respectively. The enzyme forms an α/β fold similar to bacterial cytidine deaminase, but with no similarity to the α/β barrel fold used by bacterial cytosine deaminase or mammalian adenosine deaminase. The structures observed for bacterial, fungal, and mammalian nucleic acid deaminases represent an example of the parallel evolution of two unique protein folds to carry out the same reaction on a diverse array of substrates.

Introduction

The pyrimidine salvage pathway enables organisms to utilize exogenous pyrimidine bases and nucleosides, which are not intermediates in de novo pyrimidine synthesis. Cytosine deaminase (CD; EC 3.5.4.1) catalyzes the deamination of cytosine to uracil and ammonia (Figure 1A). Cytosine deaminase is found in bacteria and fungi, where it plays an important role in pyrimidine salvage, but is not present in mammalian cells (Nishiyama et al., 1985). A comparison of *Escherichia coli* (bCD) and *Saccharomyces cerevisiae* (yCD) cytosine deaminases reveals significant differences between the bacterial and fungal enzymes, including their primary amino acid sequence, predicted molecular mass, quaternary structure, and relative substrate specificities and affinities, indicating that they are distinct and separately evolved enzymes. The yeast enzyme is a homodimer with individual subunits comprised of 158 residues, corresponding to a mass of 35 kDa per functional oligomer (Erbs et al., 1997; Hayden et al., 1998). In contrast, the bacterial enzyme is a hexamer with individual subunits comprised of 426 residues, corresponding to a mass of approximately 300 kDa for the active enzyme complex (Austin and Huber, 1993a, 1993b; Ireton et al., 2001). The bacterial enzyme is more thermostable than its yeast counterpart (Katsuragi et al., 1987; Kievit et al., 1999; B.L.S., unpublished data).

Cells expressing cytosine deaminase are sensitive to the cytosine analog, 5-fluorocytosine (5FC) due to the enzymatic conversion of 5FC to the toxic metabolite, 5-fluorouracil (5FU) (Figure 1C). This compound and its deoxyribonucleoside, fluorodeoxyuridine (FUdR), are potent inhibitors of DNA synthesis and are widely used in cancer treatment (Dipiro et al., 1997; Morris, 1993). In addition, 5FU can be incorporated into RNA by salvage pathways and interfere with RNA function. Since most fungi express cytosine deaminase, 5FC is commonly used as an antifungal agent (Dipiro et al., 1997).

Currently, cytosine deaminase is being investigated for gene therapy applications against solid tumors due to the absence of this activity in humans (Austin and Huber, 1993a; Hirschowitz et al., 1995; Huber et al., 1993; Kievit et al., 1999; Mullen et al., 1992). Mammalian cells genetically modified to express either the *S. cerevisiae* or *E. coli* cytosine deaminase gene commit metabolic suicide following administration of 5FC. Because untransfected mammalian cells do not express CD, they are immune to 5FC treatment (Katsuragi et al., 1987). 5FU is a potent antineoplastic agent in the treatment of colon, rectal, breast, stomach, pancreatic, and lung cancers. There is evidence suggesting the yeast cytosine deaminase may be a better candidate for gene therapy applications due to its lower K_M toward 5FC (Kievit et al., 1999). The CD/5FC combination of gene and prodrug has been proven effective at controlling tumor growth in animals and is currently being evaluated in several human clinical trials (Cunningham and Nemunaitis, 2001; Freytag et al., 2002a, 2002b; Greco and Dachs, 2001).

The structure and mechanism of two separate nucleoside deaminases, adenosine deaminase and cytidine deaminase, have been well characterized through a combination of NMR and crystallographic analyses (Frick et al., 1989; Jones et al., 1989; Kurz and Frieden, 1987; Mohamedali et al., 1996; Shih and Wolfenden, 1996; Wilson et al., 1991; Xiang et al., 1997). Although both utilize a catalytic zinc ion and display similar mechanisms, the two enzymes possess unrelated protein folds and active site architectures. The reactions proceed through the stereo-specific addition of a metal-bound hydroxyl group to the substrate, forming a tetrahedral transition state intermediate that decomposes through the elimination of ammonia (Figure 1A). For both enzymes, a glutamic acid residue participates in acid-base catalysis, facilitating protonation of the pyrimidine N3 nitrogen.

The structure of *Escherichia coli* cytosine deaminase (bCD), which acts exclusively on the pyrimidine nucleobase, has recently been determined in the presence and absence of the bound mechanism-based inhibitor 4-(S)-hydroxyl-3,4-dihydropyrimidine (Ireton et al., 2002). The

*Correspondence: bstoddar@fred.fhcrc.org

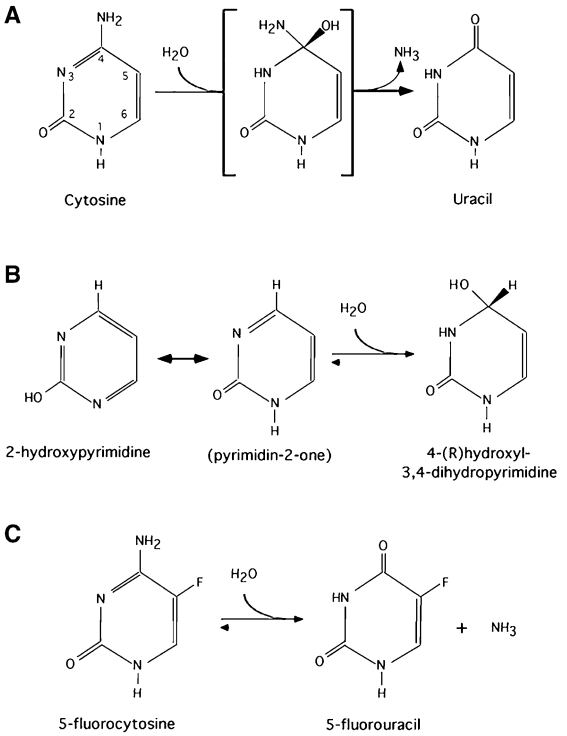

Figure 1. Cytosine Deaminase Substrates

(A) Cytosine deaminase catalyzes conversion of cytosine to uracil and ammonia. The reaction proceeds through the stereospecific addition of a metal-bound hydroxyl group to the substrate, forming a tetrahedral transition state intermediate that decomposes through the elimination of ammonia.

(B) 2-hydroxypyrimidine (also called pyrimidin-2-one in its tautomeric keto form) is enzymatically converted to a hydrated adduct that accumulates as a mechanism-based, tightly bound active site inhibitor. The structure of yCD was solved in the presence of this inhibitor as described in the text.

(C) 5-fluorocytosine is also deaminated by yCD to form 5-fluoruracil, a potent cytotoxic chemotherapy agent.

enzyme forms an $(\alpha\beta)_8$ barrel structure with structural similarity to mammalian adenosine deaminase, a relationship that is undetectable at the sequence level, and displays no similarity to bacterial cytidine deaminase. The enzyme is packed into a hexameric assembly stabilized by a domain-swapping interaction between the C terminus of enzyme subunits to form a trimer of dimers. The active site is recessed in the mouth of the enzyme barrel and contains a trigonal-bipyrimidal coordinated iron ion that coordinates a hydroxyl nucleophile. bCD is dependent on iron(II) for maximum activity, as removal of the iron(II) by treatment with *o*-phenanthroline results in inactivation of the enzyme; activity is fully restored by the addition of free iron(II) (Porter, 2000; Porter and Austin, 1993). Substitution of the active site iron(II) with zinc also restores activity, but only to approximately 10% of its maximal velocity and k_{cat}/K_M values (Porter, 2000). Substrate binding involves a significant conformational change that closes the barrel channel and completely sequesters the reaction complex from solvent.

We have now solved the structure of *Saccharomyces cerevisiae* (yCD) cytosine deaminase in the presence and absence of a mechanism-based inhibitor (4-[R]-hydroxyl-3,4-dihydropyrimidine, or DHP) at 1.4 and 1.14 Å resolution respectively, with the latter structure representing the highest resolution structure of an aminohydrolase to date. A structural comparison of yeast and bacterial cytosine deaminases reveals the enzymes have dissimilar folds, active site architectures, and bind different catalytic metal ions. A comparison of these enzymes therefore provides an example of two identical enzyme activities and specificities that have evolved independently from unique structural scaffolds.

With the structure determination of yeast cytosine deaminase, we now have high-resolution models and descriptions for the deamination of nucleobase and nucleoside substrates by both the $(\alpha\beta)_8$ barrel fold (mammalian adenosine deaminase and bacterial cytosine deaminase) and by the mixed α/β fold (bacterial cytidine deaminase and yeast cytosine deaminase). This provides the basis for a detailed analysis of the parallel, convergent evolution of identical enzyme activities with similar substrate profiles from two separate protein folds. The structure determination of bacterial and yeast cytosine deaminase will also permit comparisons of engineered enzymes that display enhanced turnover of 5-fluorocytosine, from both protein fold families. Bacterial and yeast cytosine deaminase are both under active development for anticancer prodrug gene-therapies.

Results and Discussion

Structure Determination

Yeast cytosine deaminase (yCD) was expressed in *E. coli* as an N-terminal histidine-tagged fusion construct. Removal of the histidine tag was essential for enzyme stability and crystallization (see Experimental Procedures). Crystals were obtained that belonged to space-group $P2_12_12_1$, with the asymmetric unit containing two 17.5 kDa monomers related by a noncrystallographic 2-fold axis arranged to form the physiological dimer. The structure of selenomethionine-substituted yeast cytosine deaminase was determined by the single anomalous dispersion (SAD) method at 1.4 Å resolution. Interpretable main chain electron density was observed for all 158 residues of each yCD monomer. The structure was refined to an R_{work}/R_{free} of 16.3/17.9, with 93% of residues within the most favored region for main chain phi-psi angles on a Ramachandran plot (Laskowski et al., 1993) and an average protein B factor of 9.3 $Å^2$ (Table 1). The structure of native yCD with the mechanism-based inhibitor 4-(R)-hydroxyl-3,4-dihydropyrimidine was determined to 1.14 Å and refined to an R_{work}/R_{free} of 11.0/15.2. The first three residues (Met-Val-Thr) of one of the two monomers in the asymmetric unit were disordered and omitted from the final model. The quality of the electron density map with the final model refined against data extending to 1.14 Å is shown in Figure 2.

Enzyme Fold, Oligomerization, and Active Site

The yCD monomer forms a compact domain with a mixed α/β topology containing a central β sheet ($\beta1$–$\beta5$) with two α helices ($\alpha1$ and $\alpha5$) on one side and four α helices ($\alpha2$–$\alpha4$ and $\alpha6$) on the other side of the β sheet

Table 1. Structure Determination and Refinement

	Semet-Peak	DHP-Bound yCD
Data Collection		
Wavelength (Å)	0.9795 (f″)	1.00
Resolution (Å) (outer shell)	20–1.43 (1.48–1.43)	20–1.14 (1.18–1.14)
Completeness (%)	99.9 (99.7)	92.6 (61.6)
R_{Merge}	0.042 (0.165)	0.047 (0.283)
Average I/σ (I)	27.4 (9.5)	34.3 (3.8)
Phasing power	3.3	
Figure of merit/after DM	0.52/0.86	
Refinement Statistics		
Resolution (Å)	20–1.43	10–1.14
Number reflections	51,872	92,220
Test set (5%)	2,594	4,610
R_{cryst} (%)	16.3	11.0
R_{free} (%)	17.9	15.2
Rms deviations		
Bonds (Å)	0.008	0.011
Angles (Å)	1.37	1.99
Number of protein atoms	2458	2443
Number of water molecules	391	438
Ligand atoms/bound metals	5	16/4
Average B factors (Å^2)		
Protein	9.2	9.8
Waters	19.6	20.5
Ligands		8.3

(Figures 2B and 2C). There are no extended loops on the surface of the enzyme subunit. The α5 (residue 135–148) and α6 (residue 150–156) helices are separated by a single proline residue at position 149, causing a 75° bend that redirects the α6 helix back toward the enzyme active site. The monomer dimensions are 26 × 26 × 42 Å. The yCD dimer is formed by a head-to-tail association of yCD monomers and is stabilized through stacking interactions of the α3 helices along the noncrystallographic 2-fold axis (Figure 2E). The dimer interface buries ~1000 Å^2 out of a total of 6275 Å^2 molecular surface area on each monomer. The interface is mainly hydrophobic and includes stacking interactions between identical residues within each subunit (Tyr 121A-Tyr 121B) (Figure 2A). There are also eight salt-bridge interactions made between 4 residues on each monomer, involving helix α3-loop α4-β5 (two each for Asp 92A-Arg 125B and Arg 125A-Asp 92B), and loop α2-β3-helix α6 (Arg 73A-Glu 154B and Glu 154B-Arg 73A). The overall dimer dimensions are 26 × 42 × 52 Å. The quaternary structure of yCD is completely different from that observed for the most closely related available protein structures, particularly of bacterial cytidine deaminases, as described below.

A single active site is present in each enzyme subunit, comprised of residues found on structural elements (β1, β2, α2, β3, α3, loop β4-α4, and α6) throughout the yCD monomer (Figure 2D). The active sites are separated by 14 Å and are both adjacent to the dimer interface; no cooperativity has been reported for the enzyme. The substrate binding pocket and its bound metal ions, both described below, are buried approximately 9 Å behind the mouth of the yCD active site, and are completely sequestered from exposed solvent in both the apoenzyme and substrate-bound structures. Structural elements blocking the entrance to the active site are assumed to undergo motion to allow access for substrate and binding and product release. Residues lining the entrance to the yCD active site include Phe 114 from a loop between β4 and α4, and Trp 152 and Ile 156, found on the C-terminal α6 helix. This latter helix and its residues are conserved among cytosine (but not cytidine) deaminases, and appear to be important for defining substrate specificity for the yCD enzyme subfamily.

Each active site contains a single catalytic zinc ion which is tetrahedrally coordinated by a histidine located at the beginning of helix α2 (His 62-Zn1, 2.05 Å), two cysteines on helix α3 (Cys 91-Zn1, 2.28 Å; Cys 94-Zn1, 2.31 Å), and a single bound water molecule that is appropriately positioned to act as a nucleophile in the deamination reaction ($OH_2$1-Zn1, 1.95 Å). In the absence of bound substrate or inhibitor the active site of each monomer also contains a second, noncatalytic zinc atom, which is tetrahedrally coordinated by four waters (Figure 3). The presence of the two zinc ions was confirmed by both simulated annealing omit maps and anomalous difference Fourier maps. The position of the second zinc ion and its tetrahedral coordination shell closely resembles the position, geometry, and interactions of the sp3-hybridized C4 carbon in the structure of an enzyme-bound substrate analog described below. One bound water molecule ($OH_2$1, described above) is shared between the two zinc atoms, which are 3.3 Å apart.

The noncatalytic zinc makes very short coordination to two of the four coordinating water molecules. These waters occupy strong electron density features, with one water sandwiched between the two zinc ions as described above ($OH_2$1-Zn1, 1.95 Å; $OH_2$1-Zn2, 1.73 Å), and the second water within short bonding distance to Glu 64 ($OH_2$2-Glu 64 Oδ2, 2.37 Å; $OH_2$2-Zn2, 1.75 Å). The presence of the second zinc ion is not completely

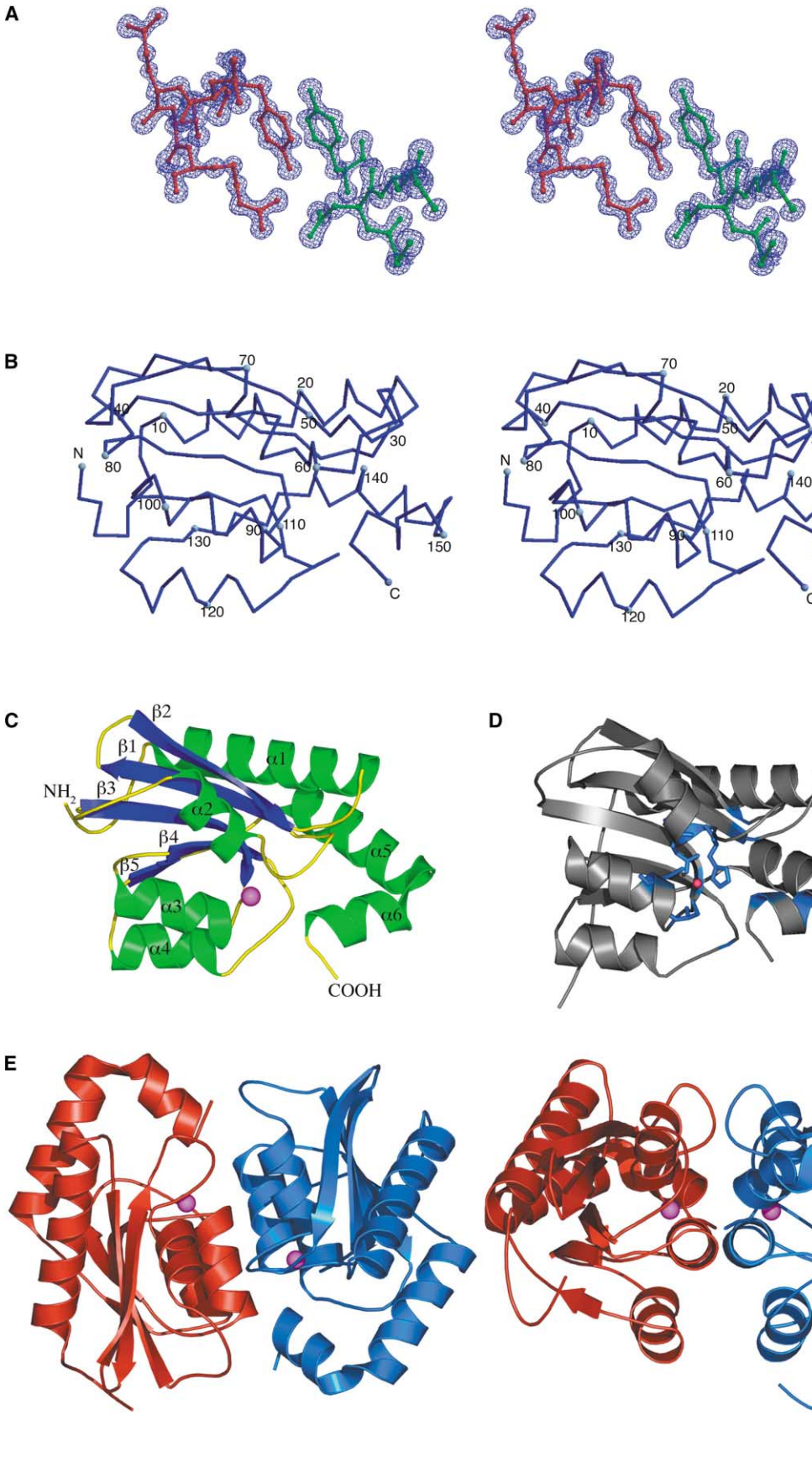
A
B
70
20
40
10
50
30
N
80
60
140
100
110
90
130
150
C
120
C
β2
β1
α1
NH2
β3
α2
β4
α5
β5
α3
α6
α4
COOH
D
E

surprising, given that 0.5 mM zinc acetate was added during protein expression induction, but was not expected given that zinc was not a buffer component during any steps of enzyme purification or crystallization, and since only one zinc has been found in the active site of adenosine and cytidine deaminases (Carlow et al., 1999; Johansson et al., 2002; Wilson et al., 1991). At this time, we assume that the presence of this bound metal ion in the apo-enzyme probably does not reflect a mechanistically relevant component of yCD catalysis but rather reflects a marked affinity for a tetrahedral center at that site that is fulfilled by the presence of exogenous zinc during protein expression. A similar, although more loosely coordinated zinc ion was also observed in one of the crystal forms of bovine carboxypeptidase A (Bukrinsky et al., 1998). In that study, an additional zinc is bound to a glutamate residue and bridged to the catalytic zinc by a hydroxyl. The second zinc acts as a competitive inhibitor, the structure mimics a "substrate bound" complex. The noncatalytic zinc observed in the yCD structure differs significantly from the inhibitory zinc bound in carboxypeptidase A in that it is not directly liganded to any protein residues.

yCD Complexed with a Mechanism-Based Inhibitor

The yCD enzyme catalyzes the deamination of a cytosine nucleobase. The reaction proceeds through the stereo-specific addition of a hydroxyl group to the cytosine substrate at the C4 position forming a tetrahedral transition state that decomposes through the elimination of ammonia to form uracil. Therefore, pyrimidine ring structures such as 2-hydroxypyrimidine, that lack an efficient leaving group for an elimination reaction at C4, are bound tightly by the enzyme and trapped as mechanism-based inhibitors with stereo-specific chiral centers at the site of the addition (Figure 1). This same reaction is well documented for other nucleic acid deaminase enzymes; a similar inhibition strategy was used in previous crystallographic studies of human adenosine deaminase (ADA), bacterial cytidine deaminase (CDA), and bacterial cytosine deaminase (bCD). For ADA, a purine ribonucleoside (nebularine) was shown to be enzymatically converted to 6R-hydroxyl-1,6-dihydropurine ribonucleoside (Wilson et al., 1991); for CDA, a pyrimidine ribonucleoside (zebularine) was used to generate a similar inhibited complex (Frick et al., 1989; Shih and Wolfenden, 1996; Xiang et al., 1997). For bCD, the inhibitor 2-hydroxypyrimidine (2HP, also called pyrimidin-2-one in its keto tautomeric form) was converted to 4-(S)-hydroxyl-3,4-dihydropyrimidine (DHP). This same compound (2HP) was used in the study of yCD reported here.

Fourier difference maps calculated using diffraction data from native yCD crystals soaked with 2HP display strong electron density for a bound 4-(R)-hydroxyl-3,4-dihydropyrimidine molecule (the opposite enantiomeric form of that seen with bCD, see below) adjacent to the catalytic zinc ion, accompanied by disappearance of the second, noncatalytic zinc (Figure 4). The electron density in these maps is consistent with the conversion of the inhibitor to a hydrated adduct that accumulates as a mechanism-based, tightly bound active site inhibitor. This species is produced by the addition of the metal-bound hydroxyl to the C4 position of the pyrimidine ring.

Three residues (Trp 152, Asp 155, and Ile 156) on the C-terminal α6 helix (noted above as being conserved in cytosine deaminase enzymes evolved with this protein fold) are in direct contact with the inhibitor molecule. The position of the residues comprising the yCD active site remain unchanged from that observed for the apo-enzyme, as the noncatalytic zinc ion and its bound water molecules occupy similar positions in the yCD binding pocket, and many of the side chains originally involved in coordinating those atoms are hydrogen bonded to the inhibitor.

There are extensive atomic interactions made between yCD side chains to every atom in the DHP ring. The following represent potential hydrogen bonds between yCD side chains and substrate atoms: Asp 155 Oδ2-DHP N1, 2.71 Å; Asn 51 Nδ2-DHP O2, 2.91 Å; Gly 63 N-DHP O2, 2.88 Å; Glu 64 Oϵ2-DHP N3, 2.80 Å; Glu 64 Oϵ1-DHP O4, 2.55 Å; and Cys 91 N-DHP O4, 3.09 Å. Observed hydrophobic interactions include: Ile 33 CD1-DHP C2, 3.26 Å; Phe 114 CE1, Leu 88 CD2, and Cys 91 CB-DHP C5, all $\sim$4.0–4.1 Å; Trp 152 CH2, CZ3-DHP C6, 4.0 Å; and Ile 156 CG2-DHP C6, 3.95 Å. In addition, the pyrimidine ring of DHP is aligned to stack with the imidazole ring of His 62.

Structural Similarity

A search of the DALI (Holm and Sander, 1993) fold recognition server reveals that the yCD monomer fold is structurally similar to three enzymes. The closest similarity (Z score 11.3; 2.6 Å superposition rmsd across 116 Cα carbons) is to the AICAR (5-aminoimidazole-4-carboxamide-ribonucleotide) transformylase domain from avian AICAR transformylase/inosine monophosphate cyclohydrolase (ATIC: PDB ID code 1G8M) (Greasley et al., 2001). This enzyme shares 9% sequence identity to yCD. Also closely similar are the cytidine deaminase folds

Figure 2. The Structure of Yeast Cytosine Deaminase

(A) Stereo view of SigmaA-weighted 2Fo-Fc electron density (blue) contoured at 2.5σ superimposed on the final refined yCD-substrate bound model showing interactions at the dimer interface (red, green).

(B) Stereo view of the yCD monomer Cα trace with every tenth residue labeled.

(C) yCD monomer ribbon diagram in the same orientation as in (B) showing a mixed α/β fold, with α helices colored green, β strands colored blue, and random coil in yellow. The catalytic Zn^{2+} ion is shown as a sphere (violet). A second Zn^{2+} ion is located adjacent to the catalytic zinc (data not shown).

(D) yCD monomer ribbon diagram in gray with the position of residues involved in substrate coordination colored blue, and side chains are shown for the catalytic residue Glu 64, and His 62, Cys 91, Cys 94 coordinating the catalytic zinc (violet).

(E) On left, top view of the yCD dimer interface, and rotated 90° (right) showing the α3 stacking helices at the dimer interface. The figure was prepared with XtalView, Raster3D, and PyMOL (DeLano, 2002; McRee, 1999; Merritt and Bacon, 1997).

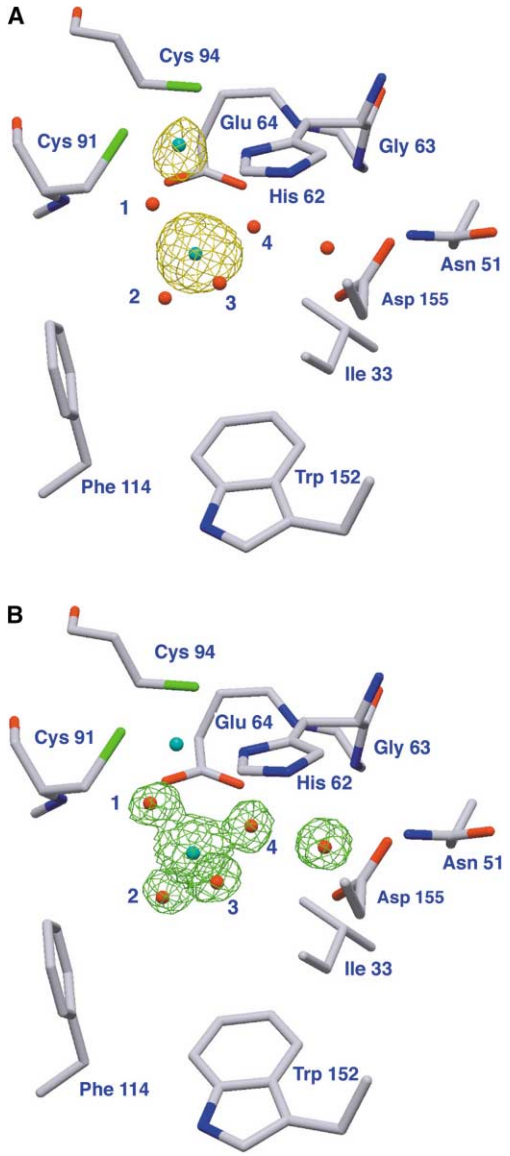

Figure 3. Noncatalytic Zinc Atom within the yCD Active Site

View of yCD apo-enzyme active site with residues colored by atom type (not shown: Leu 88, Ile 156).

(A) Anomalous Fourier synthesis map (SigmaA-weighted Fobs-Fcalc) contoured at 8σ (yellow density) showing the location of the bound Zn^{2+} ions.

(B) Fobs-Fcalc simulated annealing omit map contoured at 4σ (green density) showing the tetrahedrally coordinated noncatalytic Zn^{2+} in the absence of bound substrate. Figures 3 and 4 were made with XtalView and Raster3D (McRee, 1999; Merritt and Bacon, 1997).

from *Bacillus subtilis* (PDB 1JTK) (Johansson et al., 2002) and *Escherichia coli* (PDB 1CTT) (Betts et al., 1994), with Z scores of 9.0 and 8.0, respectively (Figure 5A). These two enzymes superimpose with the yCD monomer with rmsd values of 3.0 and 3.1 Å for superposition of 100 and 96 Cα carbons, respectively. The C-terminal AICAR transformylase domain of ATIC contains three subdomains, two of which (subdomains 2 and 4) have a similar topology. The similarity between these AICAR transformylase subdomains and *E. coli* cytidine deaminase has previously been reported (Greasley et al., 2001).

The structural similarity of the yCD monomer to the bacterial cytidine deaminase monomers noted above does not extend to the packing and architecture of the functional oligomers. *B. subtilis* CDA is a homotetrameric enzyme, while *E. coli* CDA is a homodimer. In the *E. coli* CDA structure, a pseudotetramer is formed in which two catalytic subunits are associated with two structurally homologous, noncatalytic domains lacking bound zinc, proposed to be the result of a domain duplication (Betts et al., 1994). The packing and relative orientation of subunits in the CDA tetramers is similar, giving an overall rmsd of 1.7 Å for superimposed Cα atoms from the four subunits (Johansson et al., 2002). In contrast, the complete yCD dimer cannot be superimposed on any combination of two subunits in the cytidine deaminase structures. Although mutually orthogonal noncrystallographic symmetry operators generate both the yCD dimer and the bacterial CDA oligomers, the position of these axes with respect to the enzyme subunits are different, leading to the subunit interfaces being centered around different structural elements.

Structural Comparison to Cytidine Deaminase

The active site architecture of yCD is very similar to that reported for *E. coli* and *B. subtilis* cytidine deaminase (CDA) (Figure 5B), with a highly conserved motif of residues involved in metal coordination and substrate protonation (His/Cys-X-Glu, Cys-X-X-Cys), implying a similar deamination mechanism for the deaminase family (Figure 6). There is also conservation of residues involved in the binding of nucleobases substrates. The positions of the catalytic Zn^{2+} and water molecule in yCD are structurally equivalent to the Zn^{2+} and water molecule in the CDA structures. Functionally equivalent residues involved in coordinating the bound zinc ion in yCD and *E. coli*/*B. subtilis CDA* are His 62:*His 102*/*Cys53*, Cys 91:*Cys 129*/*86*, and Cys 94:*Cys 132*/*89*. Several similar residues are also involved substrate coordination: Ile 33:*Val 73*/*26*, Glu 64:*Glu 104*/*55,* Leu 88:*Tyr 126*/*Val84*, and the main chain nitrogen of Gly 63:*Ala 103*/*54*. Three additional residues also fulfill similar roles in coordinating the bound substrate for yCD and *CDA* but are significantly displaced in the structural superposition; these residues are Asn 51:*Asn 89*/*42*, Asp 155:*Glu 91*/*44,* and Trp 152:*Phe 71*/*24*. Additional residues on adjacent subunits within the oligomeric complexes of *E. coli* and *B. subtilis* CDA contribute to the hydrophobic binding pocket observed in those structures. *E. coli* CDA uses a loop from the adjacent monomer (Phe 165-Leu 170) to sequester the hydrophobic pocket from solvent access, whereas *B. subtilis* CDA uses residues from two adjacent monomers (Tyr 48 subunit D, Phe 125 subunit B). In contrast, the yCD binding pocket is completely contained within one monomer, located behind helix α6. Though not observed, domain movements are necessary for enzyme catalysis in for both bacterial CDA and yCD.

Despite the similarities in the yCD and CDA active sites, yCD displays a high specificity for cytosine and has no reactivity toward cytidine ribonucleoside. Docking of a cytidine ribonucleoside in the yCD binding pocket results in steric clash of the ribose sugar with the α6 helix backbone and with side chains from Asn 51 and Asp 155. The decreased size of the yCD binding

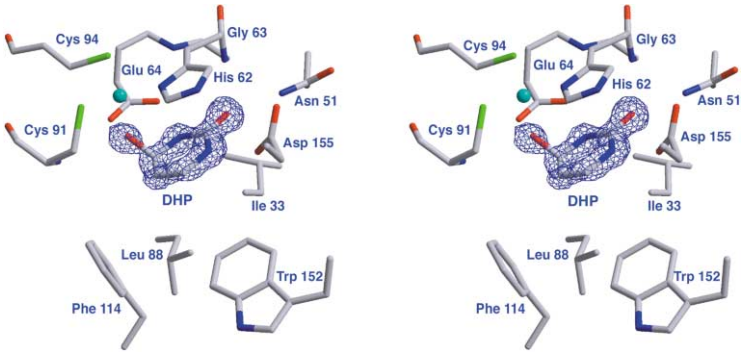

Figure 4. yCD Bound to a Mechanism-Based Inhibitor

Stereo view of yCD inhibitor-bound active site colored by atom type. Fobs-Fcalc simulated annealing omit map contoured at 4σ (blue density) showing the location of the transition state analog DHP and residues within 4Å of the bound compound (not shown: Ile 156). The map was calculated prior to the inclusion of the ligand in the crystallographic model.

pocket contributes to specificity for the hydrophobic nucleobase. Structural analysis shows this specificity results from the position of the C-terminal helix observed in the yCD monomer. The C terminus of yCD is highly conserved in amino acid sequence alignments of predicted cytosine deaminases, but is absent in alignments with known and predicted cytidine deaminases (Figure 6). Gain or loss of this C-terminal element represents a point of divergence between cytosine and cytidine deaminases with a mixed α/β fold.

Structural Comparison of Independently Evolved Nucleic Acid Deaminases

The structure of yeast cytosine deaminase is completely dissimilar from that of bacterial cytosine deaminase, though both act on the same nucleobase substrate. Yeast cytosine deaminase is a homodimer with a mixed α/β fold that displays homology to bacterial cytidine deaminase. In contrast, bacterial cytosine deaminase is a hexamer composed of individual subunits with an $(\alpha\beta)_8$ barrel fold, homologous to mammalian adenosine deaminase (Figure 7A). The coordination of the active site metal is significantly different between the two enzyme families (Figure 7B). The zinc atom in yeast cytosine deaminase is bound in a nearly perfect tetrahedral arrangement of four ligands (two cysteines, one histidine, and a bound hydroxyl ion), whereas bacterial cytosine deaminase uses an iron(II) atom coordinated in a trigonal bipyramid arrangment to five ligands (three histidines, one aspartate, and a bound hydroxyl). The mammalian adenosine deaminase enzyme (ADA) is also formed from an $(\alpha\beta)_8$ barrel scaffold and contains a catalytic zinc coordinated in a similar geometry as the iron(II) in bCD. None of the metal binding residues in bCD or ADA have structural homologs in the yCD or CDA active sites.

A common feature of both yCD and bCD is a buried active site contained within the enzyme monomer that sequesters the active site from solvent, as well as implied (yCD) or experimentally visualized (bCD) domain movements at the active site entrance during the catalytic reaction. Both enzymes make extensive contacts to substrate through a combination of hydrogen bonding

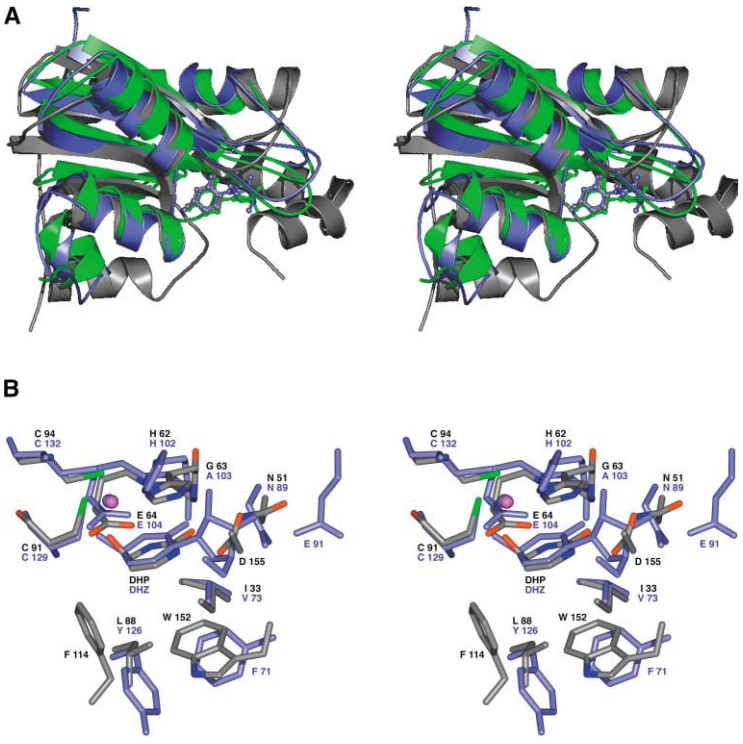

Figure 5. Superposition of Yeast Cytosine Deaminase and Bacterial Cytidine Deaminase

(A) Stereo view of a superposition (DALI) of yCD (gray) bound with 4-(R)-hydroxyl-3,4-dihydropyrimidine (DHP, gray), *E. coli* CDA (1CTT, slate) bound with 3,4-dihydrozebularine (DHZ, slate), and *B. subtilis* (1JTK, green) bound with 3,4,5,6-tetrahydro-2-deoxyuridine (THU, green) shown in ribbon diagram with bound compounds as ball and stick.

(B) Stereo view of active site residues for yCD and *E. coli* CDA with bound substrates, shown in a stick representation with yCD colored by atom type with residue labels in black, with corresponding residues and labels in CDA displayed in slate.

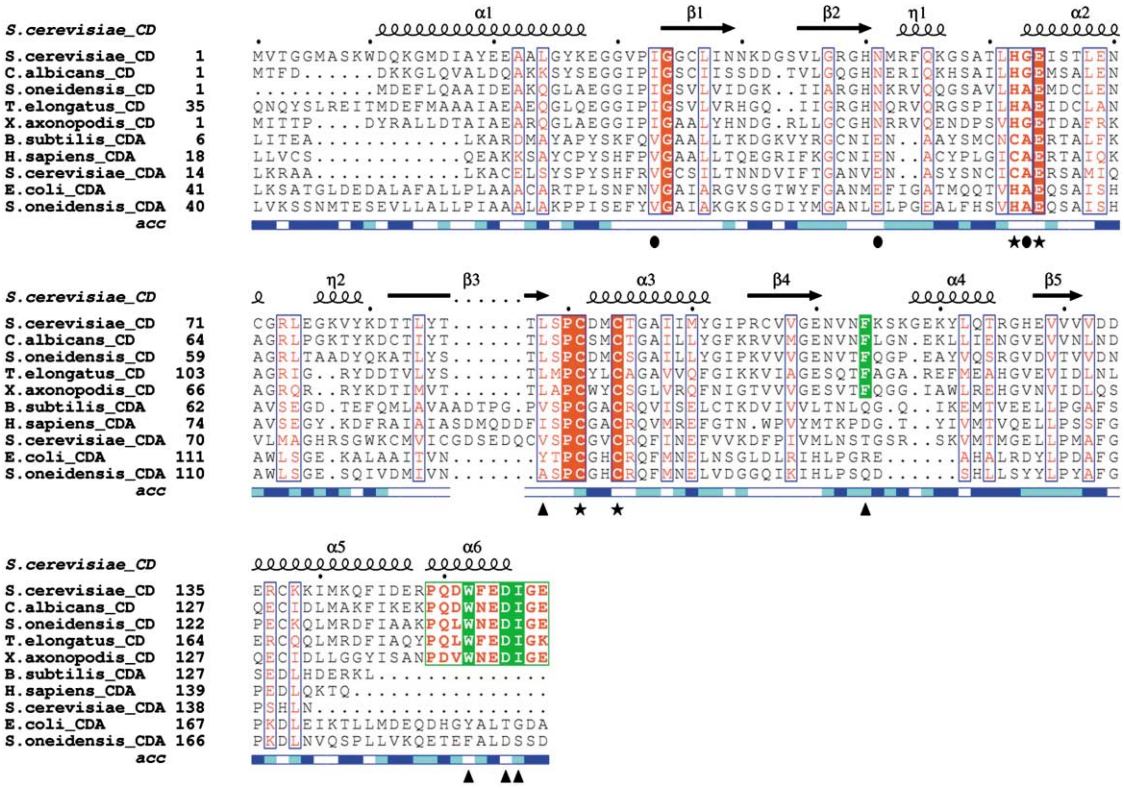

Figure 6. Sequence Alignment of Cytosine and Cytidine Deaminases

Multiple sequence alignment of five cytosine deaminases (*Saccharomyces cerevisiae*, CAA95006; *Candida albicans*, AAC15782; *Shewanella oneidensis* MR-1, AAN54462; *Thermosynechococcus elongatus* BP-1, NP_681249; *Xanthomonas axonopodis*, NP_640992), three tetrameric cytidine deaminases (*Bacillus subtilis*, P19079; *Homo sapiens*, AAB24946; *Saccharomyces cerevisiae*, ADD04031), and the catalytic domain of two dimeric cytidine deaminases (*Escherichia coli*, P13652; *Shewanella oneidensis* MR-1, AAN55813) using ClustalW (Thompson et al., 1994) and ESPript (Gouet et al., 1999). Symbols note conserved residues important for metal binding and catalysis (star), residues shared between CD and CDA substrate binding (oval), and substrate binding residues specific to CD (triangle). The bar at the bottom displays the relative accessibility of each residue for yCD, as calculated by DSSP (Kabsch and Sander, 1983). Blue indicates an accessible residue, cyan indicates a residue with intermediate accessibility, and white indicates a buried residue.

and hydrophobic interactions. While the residues lining the active site are largely different, both enzymes use a glutamate residue for protonation during catalysis. In yCD, only one carboxylate residue is present (Glu64) to abstract a proton from the zinc bound water and to protonate the N3 on the pyrimidine ring and reduce the N3-C4 double bond character for the formation of the tetrahedral intermediate. In contrast, bCD appears to use two residues for proton extraction from the metal bound water (Asp 314) and protonation of N3 on the pyrimdine ring (Glu 217). The orientation of these residues within the respective active sites leads to opposite enantiomeric conformations of the mechanism-based inhibitor (4 [R/S]-hydroxyl-3,4-dihydropyrimidine).

Conclusions

It would appear that aminohydrolase enzymes have evolved independently at least twice from separate protein fold lineages, and that binding and catalysis by either family is not uniformly correlated with the chemical differences between purine or pyrimidine, nucleobase or nucleoside, or DNA or RNA substrates. One deaminase family containing yeast cytosine deaminase and cytidine ribonucleoside deaminase evolved from a common mixed α/β ancestor. This protein fold family also appears to encompass RNA-editing adenosine deaminases (which bind and act on double-stranded RNA substrates) (Gerber and Keller, 2001). The second family evolved from an $(\alpha\beta)_8$ barrel-containing ancestor, contains both bacterial cytosine nucleobase deaminase and adenosine ribonucleoside deaminase.

Currently, both bacterial and yeast cytosine deaminase are under active development for anticancer prodrug gene therapies (Cunningham and Nemunaitis, 2001; Erbs et al., 2000; King et al., 2002; Zhang et al., 2003). The determination of the structures of yCD and bCD sets the stage for comparative studies of enzyme variants, derived from each protein fold, that display increased binding and turnover of 5FC, for the purpose of antitumor-targeted gene therapy. In this clinical strategy, tumor cells are transfected with a "suicide" gene that encodes a metabolic enzyme capable of converting a nontoxic prodrug into a potent cytotoxin (Greco and Dachs, 2001). Treatment with the prodrug allows selective eradication of tumor cells while sparing normal tissue from significant cell killing. The therapeutic effect in the tumor bed is dictated by several variables, including the efficiency of prodrug turnover.

The comparison of yCD and bCD active sites explains the higher affinity for the alternate substrate 5FC ob-

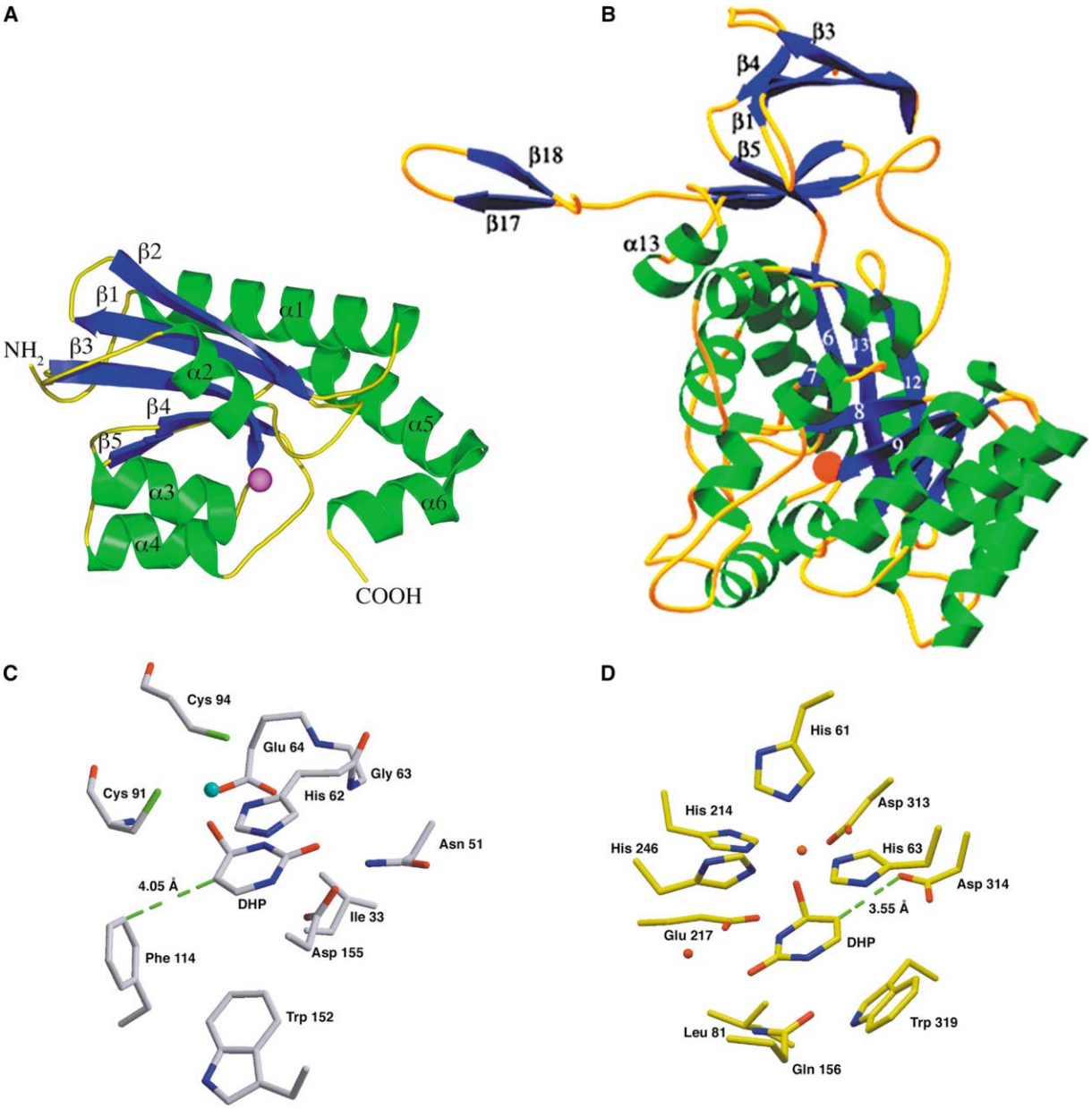

Figure 7. Structural Comparison of Yeast and Bacterial Cytosine Deaminase

Ribbon diagram for monomeric structures with α helices colored green, β strands colored blue, and random coil in yellow, and catalytic ions (yCD Zn^{2+}, violet; bCD Fe^{2+}, red) for (A) yCD and (B) bCD (prepared with Ribbons) (Carson, 1997). The bCD $(\alpha\beta)_8$ barrel is the lower domain; the bound metal ion (red sphere) is visible at one end of the barrel pore axis. The N- and C-terminal ends of the protein fold together to form the β sandwich domain (top of the ribbon diagram) and a domain-swapped C-terminal arm that participates in dimerization. Helices α1 and α8 protrude from the barrel fold and form flaps that border the entrance to the enzyme active site. Active site comparison of (C) yCD and (D) bCD bound with DHP, shown in stick representation. Dashed lines represent the nearest contact of active site residues to the C5 atom on the pyrimidine ring.

served for the yeast enzyme (Kievit et al., 1999). In yCD, the nearest protein side chain to the C5 carbon on DHP is hydrophobic (Phe 114, 4.0 Å), whereas in bCD it is electronegative (Asp 314, 3.6 Å). The presence of fluorine on the C5 carbon of the pyrimidine ring would therefore be less tolerated for bCD due to electrostatic repulsion. Mutation of bCD Asp 314 to alanine results in a 10-fold increase in 5FC turnover for the bCD enzyme (our unpublished data). Because bacterial and yeast cytosine deaminase differ dramatically in size, sequence, oligomeric packing, thermal stability, and kinetic parameters while catalyzing the same reaction, these studies will provide significant insight into the relative aspects of protein structure and function that are crucial for gene therapy applications.

Experimental Procedures

Cloning and Expression

Polymerase chain reaction was used to amplify the FCY1 gene (yCD) from pRS306-FCY1, a kind gift from Dr. Jean Emmanuel Kurtz and

Dr. Richard Jund (Strasbourg, France), to introduce an NcoI site at the start codon (Erbs et al., 1997). A 490 bp NcoI/HinDIII fragment containing the yCD gene was subcloned into pETHT restricted with the same enzymes. The resulting plasmid was confirmed by sequencing and designated pETHT:yCD. This plasmid was obtained from Margaret Black and subcloned into pET15b (Novagen, Darmstadt, Germany) using XbaI-XhoI and transformed into *E. coli* strain BL21-RIL(DE3) (Novagen). Cells expressing pET15b-yCD were grown in Luria broth media at 37°C to an OD_{600} of 0.7, induced with 0.5 mM IPTG and supplemented with 0.5 mM zinc acetate, and grown overnight at 16°C. The cells were harvested by centrifugation at 2000 × g for 10 min at 4°C, and the cell pellets were resuspended in 50 ml lysis buffer (300 mM NaCl, 20 mM Tris-HCl, pH 7.0, 5 mM Imidazole, 0.2% Triton X-100, 0.5 mM PMSF) and lysozyme added to 0.5 mg/ml, followed by 30 min incubation on ice. Cells were sonicated using a Branson Sonifier 250 equipped with a macrotip set to pulse for 5–8 min at 4°C with the duty cycle set to 40%. The cell lysate was clarified by centrifugation at 20,000 × g for 30 min at 4°C, and the clarified supernatant was passed through a 0.45 μm syringe filter.

The filtered supernatant was added to 5 ml packed bed volume of TALON metal affinity resin (Clontech, Palo Alto, CA) equilibrated with 10 bed volumes of lysis buffer, and incubated at 22°C for 30 min with rocking at 10 rpm. The affinity resin was washed 3× with 10 bed volumes wash buffer (300 mM NaCl, 20 mM Tris-HCl, pH 7.0, 10 mM Imidazole, 0.5 mM PMSF), and the YCD protein was eluted from the resin with 3 × 15 ml elution buffer (150 mM NaCl, 100 mM Imidazole, 20 mM Tris-HCl, pH 8.0). The eluted fractions were pooled and concentrated using an Amicon pressure cell with a 10 kDa cutoff and dialyzed into cleavage buffer (150 mM NaCl, 20 mM Tris-HCl, pH 8.3). Thrombin cleavage of the N-terminal histidine tag was conducted for 2 hr at 23°C using 0.5 U biotinlyated thrombin (Novagen) per milligram yCD protein in thrombin cleavage buffer (150 mM NaCl, Tris-HCl, pH 8.3, 2.5 mM $CaCl_2$). Biotinylated thrombin was removed by 30 min incubation at 23°C with 20 μl streptavidin-conjugated agarose beads (Novagen) per unit thrombin followed by gravity flow through column purification. Cleaved yCD was loaded onto to a Superdex 200 HiLoad16/60 sizing column (Pharmacia, Uppsala, Sweden) equilibrated with 50 mM NaCl, 25 mM Tris-HCl, pH 7.5, and 1 mM EDTA. Peak yCD fractions were analyzed by SDS-PAGE, then pooled and concentrated to 10–15 mg/ml, with yields of 30–45 mg of yCD (~99%) obtained per liter of bacterial culture.

For production of selenomethionine derivitized protein (Semet-yCD), pET15b-yCD was expressed in minimal media from *E. coli* strain in BL21-RIL (DE3) adapted for growth with methionine pathway inhibition (Doublie, 1997). Cells were grown in minimal media at 37°C to an OD_{600} of 0.7, and the following amino acids were added to inhibit methionine biosynthesis: lysine, 100 mg/l; threonine, 100 mg/l; phenylalanine, 100 mg/l; leucine, 50 mg/l; isoleucine, 50 mg/l; valine, 50 mg/l; and selenomethionine, 75 mg/l. Following 15 min incubation at 37°C, isopropyl-thio-β-D-galactosidase (IPTG) was added to a final concentration of 0.5 mM and the media supplemented with 0.5 mM zinc acetate, and the cultures were grown at 16°C overnight. Semet-yCD was purified analogous to native yCD. Incorportion of selenium was verified by MALDI-TOF mass spectrometry.

Crystallization and Structure Determination

An initial crystal form of yCD was grown from Hampton II sparse matrix screens in 30% PEG 8000, 0.2 M sodium acetate, and 0.1 M sodium cacodylate, by the method of vapor diffusion in hanging drops at 4°C. Crystallization was highly irreproducible, and further yCD crystals could only be obtained by microseeding into preequilibrated drops containing 2 μl of yCD protein solution at 10 mg/ml mixed with 1 μl reservoir solution consisting of 22%–25% PEG 8000, 0.2 M sodium acetate, and 0.1 M sodium cacodylate. Crystals grown in this way diffracted to ~2.0 Å, but were highly anisotropic (1.6–2.4 Å) and had high mosaicity (~1.0°). Streak seeding crystals grown in 22%–25% PEG 8000, 0.2 M sodium acetate, 0.1 M sodium cacodylate into 22%–25% PEG 8000, 0.1 M sodium cacodylate (pH 6.5), and 0.1 M calcium acetate lead to a dramatic improvement in both crystal and diffraction quality. Crystals grew as large 0.1 × 0.15 × 0.3 mm rods in 5–7 days, and diffracted to >1.1 Å with low mosaicity (0.25°) and no anisotropy. Crystals were flash cooled for data collection after sequential transfers in buffer containing 5% DMSO to a final artificial mother liquor containing 25% DMSO, 25% PEG 8000, 0.1 M sodium cacodylate (pH 6.5), and 0.1 M calcium acetate.

X-ray diffraction data for the initial structure determination were collected to 1.4 Å resolution, with spots visible to at least 1.1 Å, from crystals containing selenomethionine-derivatized protein at beam line 5.0.2 at the ALS (Advanced Light Source, Lawrence Berkeley Laboratory, Berkeley, CA) using a four panel ADSC CCD area detector. Data were collected at a wavelength corresponding to the selenium K-edge (peak) in order to determine the structure of the enzyme using the single anomalous dispersion (SAD) technique (Hendrickson, 1991). The crystals belong to the space group $P2_12_12_1$, with unit cell parameters a = 53.48 Å, b = 70.50 Å, c = 71.70 Å. The asymmetric unit contained a dimer giving a Matthews coefficient V_M of approximately 1.95 $Å^3/Da^{-1}$, corresponding to a solvent content of 35% (Matthews, 1968).

Data were processed and scaled using the DENZO/SCALEPACK program packages (Otwinowski, 1993; Otwinowski and Minor, 1997). The 14 selenium sites in the asymmetric unit were determined, and experimental phases calculated and refined, using program CNS with a random 5% of the data excluded for the purpose of cross-validation (Brunger, 1993; Brunger et al., 1998). Statistics from phasing and refinement are provided in Table 1. The initial electron density map was easily interpretable, and all 158 residues of each monomer within the asymmetric unit were manually built using XtalView (McRee, 1999). Electron density corresponding for 3 residues (Gly-Ser-Ser) remaining on the yCD N terminus after thrombin cleavage of the N-terminal histidine tag was also observed for one of the two monomers. The structure was refined using CNS, with a random 5% of the data excluded for the purpose of cross-validation to an R_{work}/R_{free} of 16.3/17.9 (Brunger, 1993).

Native yCD crystals containing the bound DHP were grown by streak seeding into preequilibrated drops as described above, with 25 mM DHP present in the well solution. X-ray diffraction data were collected to 1.14 Å (half corner) at ALS beamline 5.0.2. Data were processed and scaled using the DENZO/SCALEPACK program packages, and refined using CNS to a resolution of 1.5 Å, giving an R_{work}/R_{free} of 17.5/19.8. The model was refined against data from 10 to 1.14 Å resolution using SHELX (Sheldrick and Schneider, 1997), with the inclusion of individual anisotropic B factors, modeling multiple conformations for 16 side chains, and the placement of hydrogens, to give a final R_{work}/R_{free} of 11.0/15.2.

Acknowledgments

We acknowledge the assistance of Roland Strong, Adrian Ferre-D'Amare, and the Stoddard laboratory in the structure determination. Funding was provided by NIH grants GM49857 (to B.L.S.), CA85939 (to M.E.B.), and NCI training grant T32 CA 09437 (to G.C.I.).

Received: February 28, 2003
Revised: April 4, 2003
Accepted: May 27, 2003
Published: August 5, 2003

References

Austin, E.A., and Huber, B.E. (1993a). A first step in the development of gene therapy for colorectal carcinoma: cloning, sequencing, and expression of Escherichia coli cytosine deaminase. Mol. Pharmacol. *43*, 380–387.

Austin, E.A., and Huber, B.E. (1993b). Localization of the codA gene on the Escherichia coli chromosome. J. Bacteriol. *175*, 3685–3686.

Betts, L., Xiang, S., Short, S.A., Wolfenden, R., and Carter, C.W., Jr. (1994). Cytidine deaminase. The 2.3 A crystal structure of an enzyme: transition-state analog complex. J. Mol. Biol. *235*, 635–656.

Brunger, A.T. (1993). Assessment of phase accuracy by cross validation: the free R value. Methods and applications. Acta Crystallogr. D Biol. Crystallogr. D *49*, 24–36.

Brunger, A.T., Adams, P.D., Clore, G.M., DeLano, W.L., Gros, P., Grosse-Kunstleve, R.W., Jiang, J.S., Kuszewski, J., Nilges, M., Pannu, N.S., et al. (1998). Crystallography & NMR system: a new software suite for macromolecular structure determination. Acta Crystallogr. D Biol. Crystallogr. *54*, 905–921.

Bukrinsky, J.T., Bjerrum, M.J., and Kadziola, A. (1998). Native carboxypeptidase A in a new crystal environment reveals a different conformation of the important tyrosine 248. Biochemistry *37*, 16555–16564.

Carlow, D.C., Carter, C.W., Jr., Mejlhede, N., Neuhard, J., and Wolfenden, R. (1999). Cytidine deaminases from B. subtilis and E. coli: compensating effects of changing zinc coordination and quaternary structure. Biochemistry *38*, 12258–12265.

Carson, M. (1997). Ribbons. Methods Enzymol. *277*, 493–505.

Cunningham, C., and Nemunaitis, J. (2001). A phase I trial of genetically modified Salmonella typhimurium expressing cytosine deaminase (TAPET-CD, VNP20029) administered by intratumoral injection in combination with 5-fluorocytosine for patients with advanced or metastatic cancer. Protocol no: CL-017. Version: April *9*, 2001. Hum. Gene Ther. *12*, 1594–1596.

DeLano, W.L. (2002). The PyMOL Molecular Graphics System (San Carlos, CA: DeLano Scientific).

Dipiro, J.T., Talbert, R.L., Yee, G.C., Matzke, G.R., and Wells, B.G. (1997). Pharmacology. A Pathophysiologic Approach, Third Edition (Stamford, CT: Appleton and Lange).

Doublie, S. (1997). Preparation of selenomethionyl proteins for phase determination. Methods Enzymol. *276*, 523–530.

Erbs, P., Exinger, F., and Jund, R. (1997). Characterization of the Saccharomyces cerevisiae FCY1 gene encoding cytosine deaminase and its homologue FCA1 of Candida albicans. Curr. Genet. *31*, 1–6.

Erbs, P., Regulier, E., Kintz, J., Leroy, P., Poitevin, Y., Exinger, F., Jund, R., and Mehtali, M. (2000). In vivo cancer gene therapy by adenovirus-mediated transfer of a bifunctional yeast cytosine deaminase/uracil phosphoribosyltransferase fusion gene. Cancer Res. *60*, 3813–3822.

Freytag, S.O., Khil, M., Stricker, H., Peabody, J., Menon, M., DePeralta-Venturina, M., Nafziger, D., Pegg, J., Paielli, D., Brown, S., et al. (2002a). Phase I study of replication-competent adenovirus-mediated double suicide gene therapy for the treatment of locally recurrent prostate cancer. Cancer Res. *62*, 4968–4976.

Freytag, S.O., Paielli, D., Wing, M., Rogulski, K., Brown, S., Kolozsvary, A., Seely, J., Barton, K., Dragovic, A., and Kim, J.H. (2002b). Efficacy and toxicity of replication-competent adenovirus-mediated double suicide gene therapy in combination with radiation therapy in an orthotopic mouse prostate cancer model. Int. J. Radiat. Oncol. Biol. Phys. *54*, 873–885.

Frick, L., Yang, C., Marquez, V.E., and Wolfenden, R. (1989). Binding of pyrimidin-2-one ribonucleoside by cytidine deaminase as the transition-state analogue 3,4-dihydrouridine and the contribution of the 4-hydroxyl group to its binding affinity. Biochemistry *28*, 9423–9430.

Gerber, A.P., and Keller, W. (2001). RNA editing by base deamination: more enzymes, more targets, new mysteries. Trends Biochem. Sci. *26*, 376–384.

Gouet, P., Courcelle, E., Stuart, D.I., and Metoz, F. (1999). ESPript: analysis of multiple sequence alignments in PostScript. Bioinformatics *15*, 305–308.

Greasley, S.E., Horton, P., Ramcharan, J., Beardsley, G.P., Benkovic, S.J., and Wilson, I.A. (2001). Crystal structure of a bifunctional transformylase and cyclohydrolase enzyme in purine biosynthesis. Nat. Struct. Biol. *8*, 402–406.

Greco, O., and Dachs, G.U. (2001). Gene directed enzyme/prodrug therapy of cancer: historical appraisal and future prospectives. J. Cell. Physiol. *187*, 22–36.

Hayden, M.S., Linsley, P.S., Wallace, A.R., Marquardt, H., and Kerr, D.E. (1998). Cloning, overexpression, and purification of cytosine deaminase from Saccharomyces cerevisiae. Protein Expr. Purif. *12*, 173–184.

Hendrickson, W.A. (1991). Determination of macromolecular structures from anomalous diffraction of synchrotron radiation. Science *254*, 51–58.

Hirschowitz, E.A., Ohwada, A., Pascal, W.R., Russi, T.J., and Crystal, R.G. (1995). In vivo adenovirus-mediated gene transfer of the Escherichia coli cytosine deaminase gene to human colon carcinoma-derived tumors induces chemosensitivity to 5-fluorocytosine. Hum. Gene Ther. *6*, 1055–1063.

Holm, L., and Sander, C. (1993). Protein structure comparison by alignment of distance matrices. J. Mol. Biol. *233*, 123–138.

Huber, B.E., Austin, E.A., Good, S.S., Knick, V.C., Tibbels, S., and Richards, C.A. (1993). In vivo antitumor activity of 5-fluorocytosine on human colorectal carcinoma cells genetically modified to express cytosine deaminase. Cancer Res. *53*, 4619–4626.

Ireton, G.C., Black, M.E., and Stoddard, B.L. (2001). Crystallization and preliminary X-ray analysis of bacterial cytosine deaminase. Acta Crystallogr. D Biol. Crystallogr. *57*, 1643–1645.

Ireton, G.C., McDermott, G., Black, M.E., and Stoddard, B.L. (2002). The structure of Escherichia coli cytosine deaminase. J. Mol. Biol. *315*, 687–697.

Johansson, E., Mejlhede, N., Neuhard, J., and Larsen, S. (2002). Crystal structure of the tetrameric cytidine deaminase from Bacillus subtilis at 2.0 Å resolution. Biochemistry *41*, 2563–2570.

Jones, W., Kurz, L.C., and Wolfenden, R. (1989). Transition-state stabilization by adenosine deaminase: 1,6-addition of water to purine ribonucleoside, the enzyme's affinity for 6-hydroxy-1,6-dihydropurine ribonucleoside, and the effective concentration of substrate water at the active site. Biochemistry *28*, 1242–1247.

Kabsch, W., and Sander, C. (1983). Dictionary of protein secondary structure: pattern recognition of hydrogen-bonded and geometrical features. Biopolymers *22*, 2577–2637.

Katsuragi, T., Sakai, T., and Tonomura, K. (1987). Implantable enzyme capsules for cancer chemotherapy from bakers' yeast cytosine deaminase immobilized on epoxy-acrylic resin and urethane prepolymer. Appl. Biochem. Biotechnol. *16*, 61–69.

Kievit, E., Bershad, E., Ng, E., Sethna, P., Dev, I., Lawrence, T.S., and Rehemtulla, A. (1999). Superiority of yeast over bacterial cytosine deaminase for enzyme/prodrug gene therapy in colon cancer xenografts. Cancer Res. *59*, 1417–1421.

King, I., Bermudes, D., Lin, S., Belcourt, M., Pike, J., Troy, K., Le, T., Ittensohn, M., Mao, J., Lang, W., et al. (2002). Tumor-targeted salmonella expressing cytosine deaminase as an anticancer agent. Hum. Gene Ther. *13*, 1225–1233.

Kurz, L.C., and Frieden, C. (1987). Adenosine deaminase converts purine riboside into an analogue of a reactive intermediate: a 13C NMR and kinetic study. Biochemistry *26*, 8450–8457.

Laskowski, R.J., Macarthur, M.W., Moss, D.S., and Thornton, J.M. (1993). PROCHECK: a program to check the stereochemical quality of protein structures. J. Appl. Crystallogr. *26*, 283–290.

Matthews, B.W. (1968). Solvent content of protein crystals. J. Mol. Biol. *33*, 491–497.

McRee, D.E. (1999). A versatile program for manipulating atomic coordinates and electron density. J. Struct. Biol. *125*, 156–165.

Merritt, E.A., and Bacon, D.J. (1997). Raster3D: photorealistic molecular graphics. Methods Enzymol. *277*, 505–524.

Mohamedali, K.A., Kurz, L.C., and Rudolph, F.B. (1996). Site-directed mutagenesis of active site glutamate-217 in mouse adenosine deaminase. Biochemistry *35*, 1672–1680.

Morris, S.M. (1993). The genetic toxicology of 5-fluoropyrimidines and 5-chlorouracil. Mutat. Res. *297*, 39–51.

Mullen, C.A., Kilstrup, M., and Blaese, R.M. (1992). Transfer of the bacterial gene for cytosine deaminase to mammalian cells confers lethal sensitivity to 5-fluorocytosine: a negative selection system. Proc. Natl. Acad. Sci. USA *89*, 33–37.

Nishiyama, T., Kawamura, Y., Kawamoto, K., Matsumura, H., Yamamoto, N., Ito, T., Ohyama, A., Katsuragi, T., and Sakai, T. (1985). Antineoplastic effects in rats of 5-fluorocytosine in combination with cytosine deaminase capsules. Cancer Res. *45*, 1753–1761.

Otwinowski, Z. (1993). Data collection and processing. In Proceedings of the CCP4 Study Weekend, L. Sawyer, N. Isaacs, and S. Bailey, eds. (Warrington, UK: SERC Daresbury Laboratory), pp. 56–62

Otwinowski, Z., and Minor, W. (1997). Processing of X-ray diffraction data collected in oscillation mode. Methods Enzymol. *276*, 307–326.

Porter, D.J. (2000). Escherichia coli cytosine deaminase: the kinetics and thermodynamics for binding of cytosine to the apoenzyme and the Zn(2+) holoenzyme are similar. Biochim. Biophys. Acta *1476*, 239–252.

Porter, D.J., and Austin, E.A. (1993). Cytosine deaminase. The roles of divalent metal ions in catalysis. J. Biol. Chem. *268*, 24005–24011.

Sheldrick, G.M., and Schneider, T.R. (1997). SHELXL: high-resolution refinement. Methods Enzymol. *277*, 319–343.

Shih, P., and Wolfenden, R. (1996). Enzyme-substrate complexes of adenosine and cytidine deaminases: absence of accumulation of water adducts. Biochemistry *35*, 4697–4703.

Thompson, J.D., Higgins, D.G., and Gibson, T.J. (1994). CLUSTAL W: improving the sensitivity of progressive multiple sequence alignment through sequence weighting, position-specific gap penalties and weight matrix choice. Nucleic Acids Res. *22*, 4673–4680.

Wilson, D.K., Rudolph, F.B., and Quiocho, F.A. (1991). Atomic structure of adenosine deaminase complexed with a transition-state analog: understanding catalysis and immunodeficiency mutations. Science *252*, 1278–1284.

Xiang, S., Short, S.A., Wolfenden, R., and Carter, C.W., Jr. (1997). The structure of the cytidine deaminase-product complex provides evidence for efficient proton transfer and ground-state destabilization. Biochemistry *36*, 4768–4774.

Zhang, M., Li, S., Nyati, M.K., DeRemer, S., Parsels, J., Rehemtulla, A., Ensminger, W.D., and Lawrence, T.S. (2003). Regional delivery and selective expression of a high-activity yeast Cytosine deaminase in an intrahepatic colon cancer model. Cancer Res. *63*, 658–663.

Accession Numbers

Coordinates for yCD apo-enzyme (PDB accession code 1OX7) and yCD complexed with 4(R)-hydroxyl-3,4-dihydropyrimidine (PDB accession code 1P6O) have been deposited into the RCSB Protein Data Bank.